An anisotropic elastoplastic model for geomaterials and numerical implementation

Mountaka Souley, Mehdi Ghoreychi, Jean-Bernard Kazmierczak, Gilles Armand, D. Seyedi

AN ANISOTROPIC ELASTOPLASTIC MODEL FOR GEOMATERIALS AND NUMERICAL IMPLEMENTATION

*M. Souley
INERIS, c/o Ecole des Mines de Nancy
Campus ARTEM, CS 14234, F-54042
Nancy, France
*(*Corresponding author: Mountaka.Souley@ineris.fr)*

M. Ghoreychi, and J.-B. Kazmierczak
INERIS, BP 2
60550 Verneuil-en-Halatte, France

G. Armand
Andra R&D
Meuse/Haute-Marne Underground Research Laboratory
55290 Bure, France

D. Seyedi
Andra R&D
92298 Chatenay-Malabry, France

AN ANISOTROPIC ELASTOPLASTIC MODEL FOR GEOMATERIALS AND NUMERICAL IMPLEMENTATION

ABSTRACT

An anisotropic constitutive model is proposed in this paper accounting for both structural anisotropy and induced anisotropic plasticity. It is assumed that the rock is composed of a matrix and of potential planes of weakness. The matrix is assumed to be linear, transversely isotropic and the plasticity is described by a non linear yield function where the parameters are deduced from the nonlinear Hoek-Brown envelopes in pre- and post-peak, and derived from the laboratory characterization. A non-associated flow rule is used with a distinction between compression and extensional stress paths, as well as the absence of volumetric strain beyond large plastic distortion.

The planes of weakness are considered as known *a priori* or assumed to be oriented perpendicular to the direction of the current minor principal stress. An elastic-perfectly plastic behavior according to the Mohr-Coulomb criterion is assumed in the planes of weakness; while the elastic part is considered as linear and transversely isotropic.

Finally, the proposed model was implemented in *FLAC*^{3D} and used to simulate triaxial compressions to provide a verification of the implementation. The applicability of the implemented model to reproduce damage (pre-peak) and/or failure developments around a circular opening is checked. The GCS drift, one of the mine-by experiments set up at the main level of the Meuse/Haute-Marne Underground Research Laboratory, is selected for this first application.

KEYWORDS

Constitutive model, structural anisotropy, induced anisotropy, numerical implementation, verification

INTRODUCTION

Numerous experimental results available in the literature indicate that most sedimentary and metamorphic rocks, such as shales and slates, display a strong anisotropy of behavior and strength. These types of rocks usually exhibit some preferentially oriented structures or possess distinct bedding planes, which results in transversely isotropic behavior at the macroscopic scale: this is particularly the case of Tournemire shale (Niandou et al., 1997) or the Callovo-Oxfordian claystone (David et al., 2005).

Based on the experimental results, various failure criteria for anisotropic materials have been proposed where a large review can be found in Duveau et al. (1998). Furthermore, various constitutive models were developed in order to approach the anisotropic mechanical behavior. These are mainly (a) the empirical models based on the theory of variational cohesion and / or friction (e.g., McLamore & Gray 1967, Saroglou et Tsiambaos 2008, Wang et Yu 2014); (b) the models built on the concept of ubiquitous joint with several planes of weakness, (c) the models where damage and/or plasticity are incorporated and formulated in the framework of irreversible thermodynamics (Pietruszczak et al., 2002, Yu et al., 2013).

Since 2000, the French National Radioactive Waste Management Agency (Andra) has been constructing an Underground Research Laboratory (URL) at Bure with intent to demonstrate the feasibility of a geological repository in the Callovo-Oxfordian claystone (COx) formation by collecting in situ experimental data. The excavation of galleries at the main level of the laboratory showed a significant fracturing induced by the excavation (Armand et al., 2014) in addition to structural or inherent anisotropy observed during the laboratory tests.

Alongside this in situ investigation program and the laboratory characterization, several developments of rheological models and their implementation in numerical codes have also been undertaken. A macroscopic isotropic visco-elastoplastic model, which accounts for the impact of induced damage and fracturing on the delayed strain rates, has already been proposed in our previous studies (Souley et al., 2011). However, this model did not allow a full explanation of the different types of observed fractures, their extension, some convergence anisotropy and ratios, or the reproduction of some *in situ* pore pressure observations.

For this purpose a macroscopic anisotropic phenomenological model (including both the structural anisotropy and the induced anisotropic plasticity) has been proposed in this paper. It consists in an extension of the implicit model for strength anisotropy implemented in ITASCA codes. The basic assumption is that the failure of an anisotropic material is due to either fracturing of bedding planes (or weakness planes) or the failure of the rock matrix. The formalism is therefore based on approaches with weakness planes commonly called “Discontinuous weakness plane” or “Ubquituous joints” (aimed to account for rock mass strength and anisotropy within large-scale continuum models, Sainsbury et al., 2008) with one of the first models was proposed by Jaeger (1960) and known as ”the single plane of weakness theory”.

BRIEF REVIEW OF THE ANISOTROPIC BEHAVIOR OF GEOMATERIALS

In the literature, many experimental studies have been conducted to study the mechanical behavior of anisotropic geomaterials characterized by a large directional dependency: existence of an anisotropy of the elastic modules and the strengths as a function of the load orientation. These results were also confirmed by the study of several materials having generally a transverse isotropy by Attwell & Sandford (1974), Niandou et al. (1997), with the main features: (a) the strength of anisotropic material depends on the stress state and the loading orientation with respect to the stratification, (b) the minimum strength is generally reached when the angle of inclination β between the major stress and the weak planes ranges from 30 to 60°, (c) the ratio of resistance in the two main directions related to the anisotropy or the ratio between the minor and major strengths are used to quantify the degree of anisotropy, (d) failure may occur in very complex ways, combining sliding and separation along the planes of weakness, and a shear band in the matrix.

Research on Callovo Oxfordian claystone by measurement of the propagation velocities of ultrasonic waves showed a structural anisotropy. The work conducted by David et al. (2005) confirms the anisotropy of the wave propagation speed. The anisotropy of both the wave propagation speed and the dynamic modules has been also observed on the mechanical laboratory tests with acoustic emissions monitoring (Sarout & Guéguen 2008).

The anisotropy of the mechanical behavior of the Callovo Oxfordian was studied by a series of tests carried out in different orientations with respect to the stratification. The results show an anisotropy of deformation modulus, with a modulus ratio $E_{//}/E_{\perp}$ between 1.05 and 1.4.

Traditional measures of modules (from compression tests) show that the anisotropy could be larger, but still less than a ratio of 2. The ratio between the strength as a function of β and the strength in the isotropic plane varies between 1 and 0.8. Results showed that the strengths in the directions parallel and perpendicular to the stratification are close and slightly higher than those measured at 45 ° with respect to the bedding plane with a ratio close to 0.8 for the majority of the performed tests. However, these results need to be confirmed by additional measures according to different mineralogy.

Models based on the concept of "Discontinuous Weakness plane" allow a description of the physical mechanism related to the process of failure. In general, an anisotropic material is viewed as an isotropic body containing some planes of weakness at the macroscopic scale. In this case the basic assumption is that the failure of the anisotropic material is due to the fracture planes as well as to the rock matrix. Assuming that the weakness planes are oriented along the cracks and based on the extension of Griffith theory, several criteria are proposed in the literature (Walsh & Brace, 1964, Hoek & Brown 1980, Hoek 1983). Generally speaking, the rock matrix is modeled by nonlinear criteria involving the three invariants of stresses, while sliding along the planes of weakness follows the Mohr-Coulomb criterion or the JRC-JCS model of Barton-Bandis (1985) developed for rock joints (Wang & Huang 2009).

The proposed model is based on the concept of ubiquitous joint and yielding may occur either in the solid or along the weak planes depending on the stress state, the orientation of the weak planes and the material properties of solid and weakness planes.

FORMULATION OF THE MODEL

In the absence of sufficient data (especially quantitative) on directional dependency of the strengths and plastic flows (hardening/softening), we firstly propose a relatively simple model that can integrate the anisotropy of the elastic behavior and that of rupture, but sufficiently generic and phenomenological so that it can be subsequently enriched on the basis of (a) new knowledge and experimental data, (b) other phenomena not taken into account here (damage in the framework of continuum damage mechanics, hydromechanical couplings, time-dependent behavior, etc.).

Case of the intact rock matrix

The rheological model proposed is based on results obtained from different laboratory characterizations. The main features of the short-term mechanical behavior observed on the samples of claystone under triaxial tests can be summarized as follows: the behavior is linear under low deviatoric stresses; the loss of linearity of stress-lateral strain curves begins approximately at 50% of the peak value of the deviator stress. Under low confining pressures, a brittle failure of the samples is observed and corresponds to the formation of a shear band inclined with respect to the sample axis. There is a strong dependence of the mechanical behavior on the confining pressure, marked by a transition from a brittle toward a ductile behavior.

It has been shown that a failure criterion based on the Hoek–Brown (1980) criterion (eq. 1) is suitable for describing the shear strength of the COx claystone and as a result an elastoviscoplastic and isotropic model was proposed (Souley et al., 2011). However, since the COx claystones in their natural state have no tectonic fractures, classical signification of the Hoek & Brown parameters cannot be used for determining the rock mass strength from the results of tests on samples (and taking into account the fracturing of rock).

$$\sigma_3 = \sigma_3 - \sqrt{-m\sigma_c\sigma_3 + s\sigma_c^{\,2}} \tag{1}$$

where σ_1 and σ_3 are major and minor (absolute value) principal stresses (compressive stresses are negative), m and s are material constants, σ_c is the value of stress reached at the initiation and peak under unconfined compressive condition.

After some manipulations, the generalization of equation (1) in the space of three stress invariants (p, q, θ) leads to the following criterion for damage initiation and peak strengths:

$$F_s^m = \frac{4}{3}\frac{\cos^2\theta}{A}q^2 + \left(\frac{\cos\theta}{\sqrt{3}} - t_c\frac{\sin\theta}{3}\right)q + p - \frac{B}{A} \tag{2}$$

where p represents the mean stress, q the generalized deviatoric stress and θ the Lode's angle, A and B are two independent parameters ($A = m\,\sigma_c$ and $B = s\,\sigma_c^{\,2}$, evaluated at the initiation and peak). The parameter t_c (≤ 1) has been introduced in order to account for a potential difference of material strength for compression and extension loading paths.

Under tensile stresses, we propose a «cutoff» of mean stress to the value of tensile strength σ_t (in triaxial condition, which is by default: B/A), this leads to following yield surface in tension:

$$F_t^m = p - \sigma_t \tag{3}$$

As shown by the experimental results, we assume that the behavior of COx claystone is transversely isotropic. Assuming that the results (small changes in strength) of tests previously discussed or Brazilian tests are representative of the strength characteristics of the rock matrix, then it follows that a quasi-isotropic failure can be considered as a first approximation of rock matrix failure. The induced anisotropy due to the change of stresses will be approximated by an assumption of the existence of a weakness plane with a certain orientation. As a result, the independent parameters A and B do not change with the loading direction.

In 2005, some complementary tests carried out on claystone samples made it possible to specify the evolution of the irreversible volumetric deformation. From these tests, it came out that the hypothesis of associated flow rule tended to over-estimate the material dilatancy. Indeed, experimental data (Chiarelli

et al., 2003; Zhang & Rothfuchs, 2004) exhibit generally a contracting behavior. At best, a dilatancy develops in the last phases of the tests according to the confining pressure. The following form of plastic potential is adopted.

$$G_s^m = \left(\frac{\cos\theta}{\sqrt{3}} - t_c \frac{\sin\theta}{3} \right) q + \beta(\gamma) p \tag{4}$$

The rate of dilatancy $\beta(\gamma)$, where γ (the internal flow variable) is the plastic distortion, varies between a minimum value β_0 and a maximum value β_m, its evolution was first proposed by Chiarelli et al. (2003) and used by many authors thereafter:

$$\beta(\gamma) = \beta_m - (\beta_m - \beta_0) e^{-b_\beta \gamma} \tag{5}$$

where b_β is the plastic flow velocity.
Finally an associated flow rule is assumed in tension.

For residual strength, the same shapes of yield function as the peak are suitable when the confining pressure does not exceed the transition stress between the ductile and softening behaviors, σ_3^{bd}. Beyond this confining pressure, residual strength coincides with the peak yield function. The needed parameters of residual strength (when $\sigma_3 < \sigma_3^{bd}$) are s_r and m_r. By default s_r is taken equal to 0 and m_r is back-calculated so that the residual strength intercepts the maximum resistance for σ_3^{bd} of confining pressure.

The strain hardening in pre-peak and strain softening in post peak are modeled as a linear change of A with respect to the internal plastic variable (from the initiation A_i to the peak A_p). We also considered a parabolic evolution of parameter B as a function of γ, with horizontal tangents at peak and the beginning of residual phase, respectively, for the hardening in pre-peak and softening in post-peak.

Case of weakness planes (induced anisotropy)

The failure criterion on the weak plane, whose orientation will be defined later, is a composite Mohr-Coulomb envelope with strength «cutoff» in tension (similar to the *FLAC*^{3D} Ubiquitous Joint Model). This is justified since we can associate each plane of weakness as a dilatant (or not) rock joint (depending on the roughness type: primary and / or secondary). At this stage, we simply consider a basic failure criterion. The projection of a state of stress on the composite envelope is controlled by a non associated flow and an associated flow rules, respectively for shear and tensile failure.

Let (s, t, n) be the local system of reference axes related to the weakness plane consisting of (s, t) and n pointing in the direction of the unit normal of this plane. The magnitude of the tangential (shear) stress component on the weak plane, and the associated shear strain variable are:

$$\tau = \sqrt{\sigma_{sn}^{\ 2} + \sigma_{tn}^{\ 2}} \quad \text{and} \quad \gamma^{wp} = \sqrt{\varepsilon_{sn}^{\ 2} + \varepsilon_{tn}^{\ 2}} \tag{6}$$

The generalized stress vector used to describe weak-plane failure has four components: σ_{ss}, σ_{tt}, σ_{nn}, τ. The components of the corresponding generalized strain vector are: ε_{ss}, ε_{tt}, ε_{nn}, γ^{wp}. The weak-plane failure criterion with a tension cutoff is expressed in terms of (σ_{nn}, τ) as follow:

$$\begin{cases} F_s^{wp} = \tau + \sigma_{nn} \tan\phi_{wp} - C_{wp} \\ F_t^{wp} = \sigma_{nn} - \sigma_{wp}^t \end{cases} \tag{7}$$

where ϕ_{wp}, C_{wp} and σ_{wp}^t are respectively the friction, cohesion and tensile strength of the weak plane.

The potential function is composed of two functions used to define shear (non associated) and tensile (associated) plastic flow, respectively:

$$\begin{cases} G_s^{wp} = \tau + \sigma_{nn} \tan\psi_{wp} \\ G_t^{wp} = \sigma_{nn} \end{cases} \tag{8}$$

where ψ_{wp} is the weak-plane dilation angle.

Several experimental studies have established a correlation between the mechanical behavior of geomaterials and their microstructure (Kranz 1983). Microscopic observations on samples of several rocks subjected to different stress levels showed that microcracks follow the deformations of extension under certain preferential directions. This phenomenon induces a dilatancy and induced anisotropy. Based on different experimental results, some authors propose that the driving force of the induced anisotropic damage could be directly related to the positive part (extension) of the total strain tensor after the spectral decomposition introduced by Orizt (1985) and supplemented by Ju (1989).

As the failure along the plane of weakness may be either in shear or in tension, it can be supposed that the weakness plane remains normal to the direction of the minor principal stress. Indeed, the fact to consider that the plane of weakness is related to the positive part of the strain tends to exclude the shear failure that may occur under a compressive loading path. In the numerical implementation, the orientation of the weakness plane (in each element) is arbitrary and corresponds to an input data to be introduced by the user. By default, the normal of weakness plane is taken as the direction of the minor principal stress.

Constitutive equations and numerical implementation

Assuming that only small strains occurred, the total strain increment $d\underline{\varepsilon}$ can be subdivided in an elastic part $d\underline{\varepsilon}^e$ and a plastic part $d\underline{\varepsilon}^p$:

$$d\underline{\varepsilon} = d\underline{\varepsilon}^e + d\underline{\varepsilon}^p \quad \text{with} \quad d\underline{\varepsilon}^p = \lambda \frac{\partial G}{\partial \underline{\sigma}} \tag{9}$$

where λ is the plastic multiplier and G is the plastic potential for shear or tensile failure, for both solid rock and weakness plane related to the induced anisotropy.

If $\underline{\underline{C}}$ represents the fourth order elastic compliance tensor for transversely isotropic geomaterial, the incremental expression of Hooke's law in terms of generalized stress and strain tensors has the form:

$$d\underline{\sigma} = \underline{\underline{C}} d\underline{\varepsilon}^e \tag{10}$$

Finally, the consistency condition $dF(\kappa, \sigma) = 0$ allows to express the stress increment as a function of total strain increment:

$$d\underline{\sigma} = \left[\underline{\underline{C}} - \frac{\left(\underline{\underline{C}} : \frac{\partial F}{\partial \underline{\sigma}} \right) \otimes \left(\underline{\underline{C}} : \frac{\partial G}{\partial \underline{\sigma}} \right)}{\frac{\partial F}{\partial \underline{\sigma}} : \underline{\underline{C}} : \frac{\partial G}{\partial \underline{\sigma}} - \frac{\partial F}{\partial \kappa} \frac{\partial G}{\partial \varpi}} \right] d\underline{\varepsilon} \tag{11}$$

where F is the yield function; κ is the accumulated plastic strain (e.g. γ for matrix failure or γ^{wp} for failure along the weakness plane); ϖ is the generalized deviatoric stress (q) for matrix failure and the tangential stress (τ) for failure along the weakness plane.

For both (rock matrix and weakness planes) failures, a function representing the diagonal between $F_s = 0$ and $F_t = 0$ is evaluated in order to select the type of failure (in shear or in tension). At each step, the computation of new stresses is achieved by testing firstly failure in the solid matrix, then along the plane of weakness. More precisely, the main procedure is summarized below.

- The first approximation of stress tensor $\underline{\sigma}^i$, is evaluated by adding to the previous stress tensor the stress increment computed from the total strain increments and the Hooke's law.
- Computation of the yield function for rock matrix, $F^m(p^i, q^i, \theta^i)$ according to eqns 2 and 3. If the stress state, $\underline{\sigma}^i$, satisfies the yield criterion: $F^m(p^i, q^i, \theta^i) > 0$, the new increment of stresses is computed as well as the new stress tensor, $\underline{\sigma}^o$. If $F^m(p^i, q^i, \theta^i) \leq 0$, the current stress components are: $\underline{\sigma}^o = \underline{\sigma}^i$.

The resulting stress tensor, $\underline{\sigma}^o$, is then examined for failure on the weak plane.

- The corresponding stress components in the local axes, $\underline{\sigma}'^o$, are computed using the transformation from global *x*-, *y*-, *z*-axes to the local system of reference *s*-, *t*-, *n*-axes.
- Computation of the yield function for weak plane, $F^{wp}(\sigma_{nn}'^o, \tau'^o)$ according to equation (6). If the stress state $\underline{\sigma}'^o$ verifies the yield criterion $F^{wp}(\sigma_{nn}'^o, \tau'^o) > 0$, the new increment of stresses is computed as well as the new stress tensor, $\underline{\sigma}^n$. If $F^{wp}(\sigma_{nn}'^o, \tau'^o) \leq 0$, the current new stresses are: $\underline{\sigma}^n = \underline{\sigma}'^o$.
- Back to global system of reference *x*-, *y*-, *z*-axes.
- Parameters depending on the internal plastic variable are updated.

This routine has been written in C++ and compiled as a Dynamic Link Library (DLL) file that can be loaded whenever it is needed.

All parameters have already been identified from triaxial tests for the short-term response (Su, 2003, Chiarelli 2003). Note that, results of laboratory tests showed a wide variability of peak and residual plastic strains, they can be viewed as calibration parameters for in situ applications. Parameters related to the failure along planes of weakness were not for the time based on a characterization campaign: the choice of the considered values is arbitrary and deserves further attention in future studies. Also for reasons of simplicity the elastic characteristics along transverse planes of weakness are considered identical to those of the matrix as by default ($E_1=E_s$, Young modulus in the isotropic (matrix) and weakness plane; $E_3=E_n$, Young modulus in the direction normal to the isotropic (matrix) and weakness plane; $G_{13}=G_{sn}$, shear modulus in the anisotropic plane; $\nu_{12}=\nu_{st}$ and $\nu_{13}=\nu_{sn}$, Poisson coefficient respectively in the isotropic and anisotropic planes). Table 1 provides the list of parameters and input values.

Table 1. Values of input parameters

Parameter	Value	Parameter	Value	Parameter	Value	Parameter	Value
$E_1=E_s$	5600 MPa	m_i	1.5	m_p	2	σ_3^{bd}	25 MPa
$E_3=E_n$	4000 MPa	s_i	1	s_p	0.128	s_r	0
$G_{13}=G_{sn}$	[(a)]	σ_{ci}	9.6 MPa	σ_{cp}	33.5 MPa	m_r(output)	2.172
$\nu_{12}=\nu_{st}$	0.3	C_{wp}	1 MPa	ϕ_{wp}	15°	γ^{peak}	$3.75\ 10^{-3}$
$\nu_{13}=\nu_{sn}$	0.25	σ_{wp}^t	1 MPa	ψ_{wp}	5°	$\gamma^{residual}$	$8.5\ 10^{-3}$
β_0	-0.1	β_m	0.3	b_β	600	t_c	1

[(a)] G_{13}=1807 MPa is computer based on the relation of Lekhnitski (1981)

VERIFICATION AND APPLICATION

Triaxial compression path

In order to verify the model (constitutive equations and numerical implementation), several triaxial compression tests with confining pressures of 0.01, 1, 5, 10, 20, and 30 MPa are simulated. Figure 1 presents the deviatoric stress – axial, lateral and volumetric strain curves for different confining pressures. The difference between predicted strengths and those obtained in laboratory tests is related to the lower values of the parameters s_i, σ_{ci}, m_i, s_p, σ_{cp}, and m_p used in this study. The lower values are appropriated for modeling of in situ structures, whereas the mean values allow to well reproduce the laboratory strengths. From figure 1a, we note that the post-peak behavior is confining pressure dependent: the transition stress between brittle failure and ductile behavior is clearly marked and with an input value of transition stress, σ_3^{bd}, about 25 MPa. The resulting curves display four regions (elastic, hardening in pre-peak, softening in post-peak and residual phases) when the confining pressure is below the transition stress level σ_3^{bd}. It displays three regions (elastic, hardening and perfect plastic phase) under high confining pressure. These curves are qualitatively similar to the experimental ones (which were not reported herein).

Figure 2 shows a comparison in terms of the elastic limit, the peak and residual strengths between the simulation (corresponding values in Figure 1) and theory (Eq. 1). A good agreement can be observed as numerical and analytical solutions coincide. More precisely, the relative error for peak strength is less than 0.1%, and 3% for the elastic limit and residual strength respectively. This validates the numerical implementation of the proposed anisotropic elastoplastic model in FLAC^{3D}.

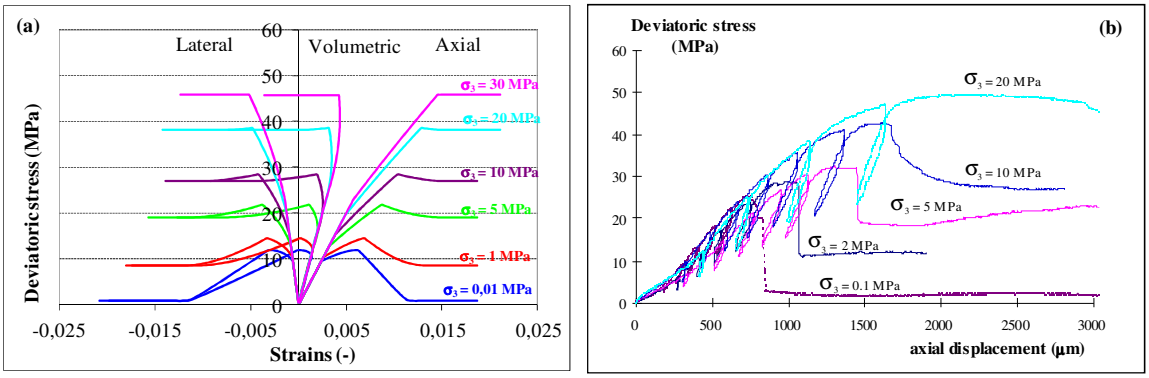

Figure 1. Triaxial compression tests: (a) numerical simulations, stress vs strains; (b) laboratory tests, stress vs axial displacement

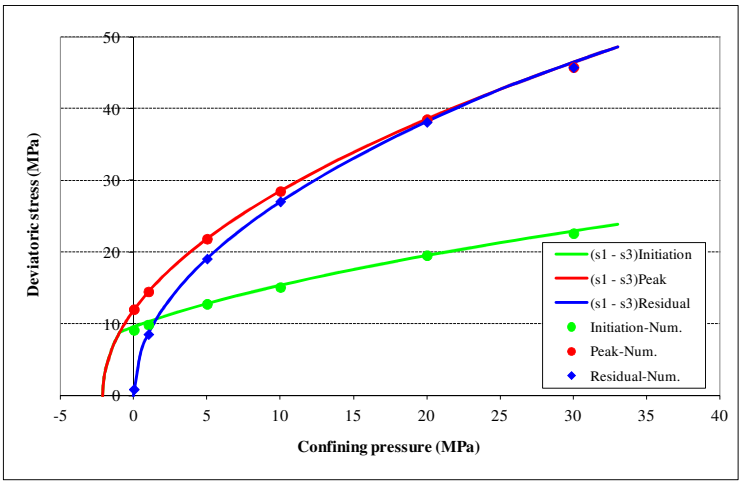

Figure 2. Elastic limit, peak and residual strengths: numerical and analytical solutions

Application to a circular opening of Meuse-Haute Marne Underground Research Laboratory

The aim of this section is to provide a verification of the implementation for non-triaxial stress paths and to show numerically the ability of the implemented model to evaluate the extent of damaged (in pre-peak) and failed (post-peak) zones around a circular underground excavation. The GCS drift excavated in the direction of the principal horizontal major stress is selected for this application. This is one of the several mine-by experiments set up at the main level -490 m of the Meuse/Haute-Marne URL where an anisotropic in situ stress state has been measured (Wileveau et al, 2007). The GCS drift has a circular section with a 2.6 m radius and can be considered as an isolated gallery.

We deliberately chose a drift oriented in the direction of the principal horizontal major stress, leaving a very low stress anisotropy ratio (between the principal minor horizontal stress and principal vertical stress) of 0.98 in the drift section and for which earlier simulations performed in the framework of the isotropic continuous approaches failed to reproduce the extension of fractured zones and the ratio of convergence observed in situ.

Taking into account the knowledge on the in situ stress state, σ_v, σ_h and σ_H are considered to be equal respectively to 12.7, 12.4 and 16.12 MPa, corresponding to the maximal stress ratio of 1.3. In the numerical model centred at the depth of 490 m, the three initial in situ stresses are distributed according to the depth. Roller displacement conditions were applied to the base of the model whereas boundary stresses (depending on the depth) were applied to the others planes (top and lateral limits of the model).

Figure 3 shows the extent of plastic zones around the circular opening. In this figure the legend "hard", "soft", "res" correspond respectively to the shear failure of the rock matrix in the pre, post peak and residual region. "Shear" and "tens" are associated to the shear and tensile failures along the plane of weakness. Plastics radius in the vertical and horizontal directions are respectively 3.4 and 5.3 m, that is to say 0.65 D and 1.02 D. These extensions are in the range of fractured (connected or not) zones extensions observed around the drifts oriented in the direction of the major horizontal stress (Armand et al., 2014).

For this instantaneous mechanical calculation, the horizontal and vertical convergences are respectively 5.2 and 4 cm, this corresponds to an initial convergence ratio of 1.3.

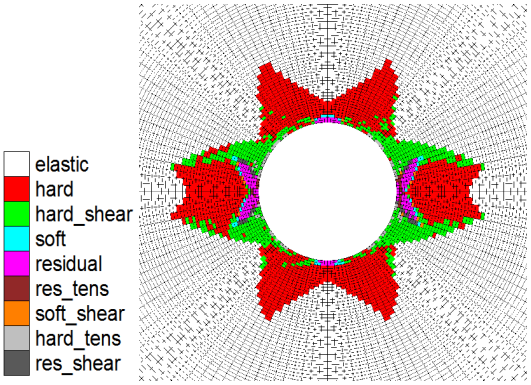

Figure 3. Extent of plastic zones around the opening

Figure 4 shows the profiles of radial, orthoradial and axial stresses along two radial lines at approximately 0° and 90° with respect to x-axis as a function of the radial distance from the gallery center. From the profile of orthoradial and axial stresses, one can distinguish different regions (elastic, pre-peak and post-peak and residual, without particular transition between the post-peak and the residual domains) through the slopes of curves. In particular at $\theta = 90°$, the first loss of slope can be noticed along the profile of orthoradial and axial stresses: the corresponding radial distance (approximately 3.4 m) is in accordance with the previous investigation of plastic zone extent. Between this radial distance and 6 m, there is a non-monotonic evolution of orthoradial and axial stresses in relation to the plastic area formed at ± 65 ° with respect to horizontal direction.

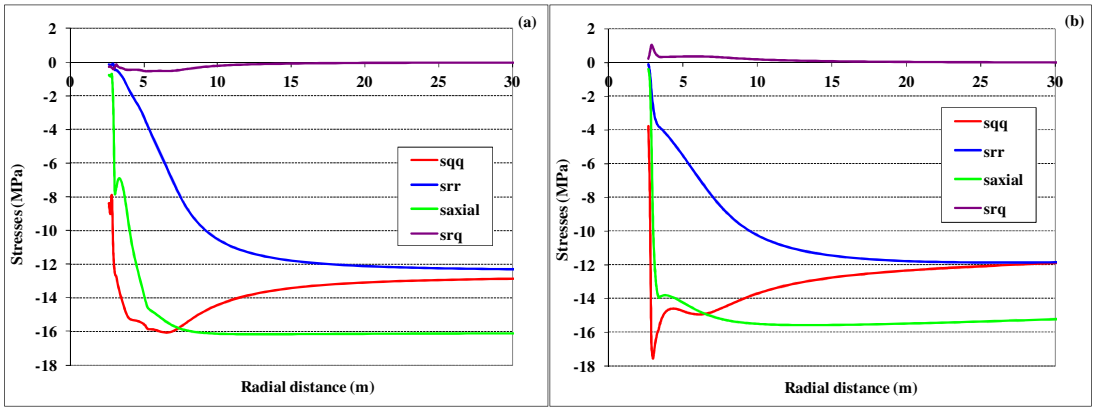

Figure 4. Radial, orthoradial, axial and shear stresses along radial lines (a) at 0° (b) at 90°

CONCLUSION

This paper presents the development of an anisotropic constitutive model for transversely isotropic geomaterials, its numerical implementation in the three-dimensional code *FLAC^{3D}*, as well as its verification and validation. Firstly, a non-linear elastoplastic model based on the interpretation of laboratory test performed using the Hoek-Brown failure criterion, is presented. The elastic anisotropy, the almost isotropy of strength observed on the available tests carried out in several directions, the induced anisotropy observed on the in situ structures are the main ingredients for this model. The rock behavior is characterized by a non-linear behavior in pre peak, a non-linear softening in post-peak and a perfectly plastic behavior in the residual phase. As observed on laboratory tests, the model takes into account the transition between the softening in post-peak under low confining pressures and the ductile behavior under high confining pressures.

Simulation of triaxial compression tests at different levels of confining pressure provides a verification of the implemented model. The resulting curves display four regions (elastic, hardening in pre-peak, softening in post-peak and residual phase) when the confining pressure is below the transition stress, and three regions (elastic, damage and perfect plastic phase) under high confining pressure. In addition, the elastic limit, the peak and residual strengths derived from these simulations are compared with the theoretical envelopes: the corresponding relative error does not exceed 1%.

The ability of the implemented model to reproduce the plastic zones around an underground drift excavated in the Callovo-Oxfordian claystone is successfully tested. The results provide new insights on the understanding of the deformation mechanisms observed around the structures of Meuse/Haute-Marne Underground Research Laboratory.

Next step will be to enrich the proposed model on the basis of new knowledge and experimental data, and/or other phenomena that have not been taken into account here (damage in the framework of damage mechanics, hydromechanical couplings, time-dependent behavior etc.).

REFERENCES

Armand, G., Leveau, F., Nussbaum, C., de La Vaissiere, R., Noiret, A., Jaeggi, D., Landrein & P. Righini, C. (2014). *Geometry and properties of the excavation induced fractures at the Meuse/Haute-Marne URL drifts.* Rock Mech. Rock Eng., 47, 21-41. doi:10.1007/s00603-012-0339-6.

Attewell, P.B., & Sandford, M. R. (1974). *Intrinsic shear strength of a brittle anisotropic rock. I: experimental and mechanical Interpretation.* Int. J. Rock Mech. Min. Sci. & Geomech. Abstr., 11, 423

Bandis, S. C., Barton, N. R. & Christianson, M. (1985). *Application of a New Numerical Model of Joint Behaviour to Rock Mechanics Problems.* in Fundamentals of Rock Joints Björkliden, Sweden, September 1985, pp. 345-356.

Chiarelli, A. S., Shao, J.F. & Hoteit, N. (2003). *Modelling of elastic-plastic damage behaviour of a claystone.* Int J Plast;19:23–45.

David, C., Robion, P. & Menendez, B. (2005). *Anisotropy of elastic, magnetic and microstructural properties of the Callovo-Oxfordian shales (Meuse).* in: 2nd Int Meeting Clays in Natural & Engineered Barriers for Radioactive Waste Confinement.

Duveau, G., Shao, J.F. & Henry, J.P. (1998). *Assessment of some failure criteria for strongly anisotropic materials.* Mech Cohes-Frict Mater;3:1–26.

Hoek, E. & Brown, E. T. (1980). *Empirical strength criterion for rock masses.* J. of the Geotech. Eng. Div., A.S.C.E., 106 (GT9), 1013.

Hoek, E. (1983). *Strength of jointed rock masses.* Geotechnique, 33 (3), 187.

Jaeger, J. C. (1960). *Shear failure of anisotropic rocks.* Geol. Mag., 97, 65.

Ju, J.W. (1989). *On energy-based coupled elastoplastic damage theories: constitutive modelling and computational aspects.* Int. J. Solids Struct. 25 (7), 803– 833.

Kranz, R. (1983). *Microcracks in rocks - a review.* Tectonophysics, 100, 117-197.

Lekhnitskii, S. G. (1981). Theory of Elasticity of an Anisotropic Body. Moscow: Mir Publishers

McLamore, R. & Gray, K. E. (1967). The *mechanical behavior of anisotropic sedimentary rocks.* J. of Engineering for Industry, Trans. of the A.S.M.E., 89, 62.

Niandou, H., Shao, J.F., Henry, J.P. & Fourmaintraux, D. (1997). *Laboratory investigation of the mechanical behavior of tournemire shale.* Int J Rock Mech Min Sci 34(1):3–16.

Pietruszczak, S., Lydzda, D. & Shao, J.F. (2002). Modeling of inherent anisotropy in sedimentary rocks. Int J of Solids and Struct, 39, 637-648.

Sainsbury, B., Pierce, M. and Mas Ivars, D. (2008). *Simulation of rock mass strength anisotropy and scale effects using a Ubiquitous Joint Rock Mass (UJRM) model.* Proc 1rst International FLAC/DEM Symposium on Numerical Modelling, 25–27 August, Minneapolis, USA, Minneapolis.

Saroglou, H. & Tsiambaos, G. (2008). A *modified Hoek–Brown failure criterion for anisotropic intact rock.* Int J Rock Mech Min Sci 45: 223–234

Sarout, J. & Guéguen, Y. (2008). *Anisotropy of elastic wave velocities in deformed shales. Part I: Experimental results.* Geophysics 73/5, D75-D89

Souley, M., Armand, G., Su, K., & Ghoreychi, M. (2011). *Modelling of the viscoplastic behaviour including damage for deep argillaceous rocks.* Physics and Chemistry of the Earth;36:1949–59.

Su, K., (2003). *Constitutive Models for the Meuse/Haute-Marne Argillites – MODEX- REP*, European Commission – Nuclear science and technology, Contract n° FIKW-CT2000-00029, 2-3.

Walsh, J. B. & Brace, J. F. (1964). A *fracture criterion for brittle anisotropic rock.* J. of Geophysical Research, 69 (16), 3449.

Wang, J. & Yu, H.-S. (2014). *Three-dimensional shakedown solutions for anisotropic cohesive frictional materials under moving surface loads.* Int. J. Numer. Anal. Meth. Geomech. 2014; 38:331–348.

Wang, T.-T., & Huang, T.-H. (2009). *A constitutive model for the deformation of a rock mass containing sets of ubiquitous joints.* Int J Rock Mech Min Sci 46 (2009) 521–530.

Wileveau, Y., Cornet, F.H., Desroches, J. & Blumling P. (2007). *Complete in situ stress determination in an argillite sedimentary formation.* Physics and Chemistry of the Earth;32(8–14):866–78.

Yu, H. D., Chen, W. Z., Li, X. L., & Sillen X. (2013). *A Transversely Isotropic Damage Model for Boom Clay.* Rock Mech Rock Eng. DOI 10.1007/s00603-012-0346-7.

Zhang, C., & Rothfuchs, T. (2004). *Experimental study of the hydro-mechanical behavior of the Callovo-Oxfordian argillite.* Applied Clay Science, 26, 325-336.